Runaway electron confinement modelling for rapid shutdown scenarios in DIII-D, Alcator C-Mod and ITER

2011 Nucl. Fusion 51 063032

(http://iopscience.iop.org/0029-5515/51/6/063032)

IOP Publishing and International Atomic Energy Agency Nuclear Fusion
Nucl. Fusion **51** (2011) 063032 (10pp) doi:10.1088/0029-5515/51/6/063032

Runaway electron confinement modelling for rapid shutdown scenarios in DIII-D, Alcator C-Mod and ITER

V.A. Izzo[1], E.M. Hollmann[1], A.N. James[1], J.H. Yu[1], D.A. Humphreys[2], L.L. Lao[2], P.B. Parks[2], P.E. Sieck[2], J.C. Wesley[2], R.S. Granetz[3], G.M. Olynyk[3] and D.G. Whyte[3]

[1] Center for Energy Research, University of California at San Diego, La Jolla, CA 92093-0424, USA
[2] General Atomics, PO Box 85608, San Diego, CA 92186-5608, USA
[3] Massachusetts Institute of Technology, Cambridge, MA, 02139-4307, USA

E-mail: izzo@fusion.gat.com

Received 17 December 2010, accepted for publication 15 April 2011
Published 20 May 2011
Online at stacks.iop.org/NF/51/063032

Abstract
MHD simulations of rapid shutdown scenarios by massive particle injection in DIII-D, Alcator C-Mod and ITER are performed in order to study runaway electron (RE) transport during mitigated disruptions. The simulations include a RE confinement model using drift-orbit calculations for test particles. A comparison of limited and diverted plasma shapes is studied in DIII-D simulations, and improved confinement in the limited shape is found due to both spatial localization and reduced toroidal spectrum in the nonlinear MHD activity. C-Mod simulations compare shutdown scenarios in which impurity (Ar) fuelling is concentrated in the edge versus the core, and the confinement of REs in the core is maintained until the onset of the $m = 1/n = 1$ mode, which is delayed in the case of edge deposition, relative to core deposition. But, the overall RE loss fraction is 100% regardless of Ar fuelling profile. A comparison of simulations across the three devices points to a trend of increased RE confinement with increasing device size, wherein all REs are lost in C-Mod, all are confined in ITER, and a partial loss is observed in DIII-D. This trend is related to a reduction in the fluctuating field amplitude near the plasma edge during the thermal-quench-induced MHD activity. The result bodes poorly for RE mitigation strategies in ITER that rely on MHD deconfinement of REs.

(Some figures in this article are in colour only in the electronic version)

1. Introduction

When a disruption occurs in a tokamak plasma, the stored thermal energy generally quenches prior to and more rapidly than the stored magnetic energy. The resulting scenario of a large plasma current carried by a relatively cold, resistive plasma produces large electric fields that can drive electrons to relativistic energies in the range of at least tens of MeV. In significant numbers, these relativistic runaway electrons (REs) have the potential to do appreciable damage to the tokamak first wall. Thus, it is desirable to devise strategies to avoid generation of large RE populations during disruptions.

The predominant mechanism for producing REs in ITER is expected to be the knock-on avalanche mechanism [1], in which new REs are created through collisions between existing REs and thermal electrons, creating an exponentially growing RE population. A 'seed' population of REs is required to initiate the avalanche; however, the total avalanche gain scales as the exponential of the initial plasma current ($G_{\mathrm{RE}} \approx \exp[2.5 I_{\mathrm{p}}(\mathrm{MA})]$), and is sufficiently large in ITER ($I_{\mathrm{p}} \sim 15\,\mathrm{MA}$), that even a very small seed from Dreicer, hot-tail, tritium decay, or other mechanism, has the potential to convert nearly all of the initial plasma current to REs [2]. The exponential growth of the RE population can potentially be thwarted if a loss mechanism exists that is comparable to or larger than the growth rate. For instance, if the confinement time of the REs is short compared with the e-folding time, the avalanche will not occur. The destruction of flux surfaces typically associated with a tokamak disruption arouses optimism in the possibility of poor RE confinement as a viable solution. In this paper we calculate the confinement of REs in the context of MHD turbulence produced during rapid shutdown scenarios (mitigated disruptions) in three tokamaks of different sizes.

Section 2 summarizes relevant RE experiments on DIII-D and C-Mod, and section 3 describes the computational model used for the simulations. The results of five simulations are presented in section 4, broken into three parts. In section 4.1 we describe two simulation of DIII-D with different plasma shapes, in order to investigate the difference between RE confinement in elongated, diverted plasmas and more circular, limited plasmas, which has been studied in DIII-D experiments. In section 4.2 two C-Mod simulations are presented with different Ar fuelling profiles to initiate the rapid shutdown (producing pellet-like or gas-jet-like shutdown scenarios). In section 4.3 an ITER simulation is presented and compared with comparable simulations of the other two devices. Finally we summarize the simulation results and discuss conclusions and implications in section 5.

2. RE experiments on DIII-D and Alcator C-Mod

In the DIII-D tokamak, a series of RE experiments have been performed in which an Ar ice pellet is injected to initiate a rapid shutdown (an intentional, mitigated disruption) of the plasma [3]. Unlike massive gas injection (MGI), which typically does not produce observable RE populations in DIII-D [4], the Ar pellet shutdowns often produce RE current plateaus of up to 400 kA or slightly higher. The production of REs by more deeply penetrating Ar pellets, but not Ar MGI, may be related either to the generation of a larger 'seed' population when more high-Z material reaches the core, or to improved confinement of the seed during thermal quench (TQ)-induced MHD fluctuations. A range of RE currents is observed in the Ar pellet experiments. In particular, in elongated, diverted DIII-D discharges, the RE plateau current can vary between hundreds of kA and effectively zero (or below observable levels) on a shot-to-shot basis, with no prescribed changes in the target discharge. This non-reproducibility creates difficulties is developing statistics related to RE mitigation methods. Low elongation, limited plasma shapes in DIII-D were found to produce RE current plateaus with significantly greater reliability, motivating a number of RE mitigation experiments in this configuration [3].

In Alcator C-Mod, rapid shutdown experiments have focused on MGI. Similar to DIII-D, MGI by itself does not produce any significant RE population in C-Mod [5]. In RE experiments, the lower hybrid current drive (LHCD) system is used to produce a significant seed population of fast electrons prior to initiating the rapid shutdown with MGI [6]. In [6], results were reported for a diverted plasma with an elongation of 1.65. Those experiments found evidence of high energy REs striking the wall during the TQ (not seen without LHCD), based on hard x-ray (HXR) and photo-neutron measurements, but no clear indication of REs surviving into the current quench (CQ) phase. More recently, these experiments were repeated on C-Mod with low elongation, limited target plasmas. An example with elongation of 1.03 appears in figure 1. Comparing these results with figure 11 from [6], we see a distinct feature that does not appear in the diverted plasmas—a signal on the HXR and photo-neutron detectors towards the end of the CQ phase, indicating a second loss event of REs which survived past the TQ phase—a possible sign of improved confinement. Still, the RE population in the CQ phase is not large enough to alter the current decay relative to the no-LHCD control discharges. Because C-Mod and DIII-D are different sized tokamaks performing substantially different RE experiments, making connections between these results, and drawing conclusions, is difficult. A major aim of the simulations described in the following sections is to isolate some of the experimental variables that may contribute to variations in RE confinement.

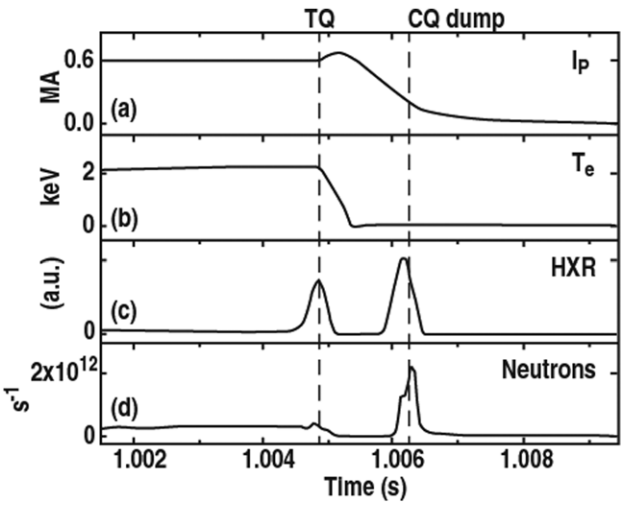

Figure 1. MGI-triggered disruption in limited C-Mod discharge (1100908026) with LHCD RE seeding. Start of TQ and end of CQ seen in (*a*) plasma current and (*b*) central electron temperature coincide with REs striking the wall as indicated by (*c*) HXR and (*d*) photo-neutron measurements.

3. Computational model

The set of simulations presented in the following sections are performed with the extended MHD code NIMROD [7]. The equations evolve the magnetic field (with a resistive-MHD Ohm law), a single fluid velocity, a single temperature and a set of continuity equations governing the deuterium ion density, and the density of each charge state (including neutrals) of an impurity species, in this case argon. The inclusion of an impurity species allows rapid shutdown techniques based on massive particle injection (MPI) to be modelled (including gas injection, pellet injection, etc). Cooling due to ionization, radiation and recombination is incorporated into the temperature evolution, while the local Z_{eff} is incorporated into the Spitzer expression for resistivity. To initiate an MPI shutdown simulation, a source of neutral impurity atoms is specified. The impurity source can entail a gradual delivery of atoms, or an instantaneous delivery, in which all of the injected atoms are deposited with a prescribed spatial distribution at $t = 0$. The latter method, while less physically realistic, can significantly reduce computational intensiveness of the simulation, and is thus used in the simulations described in the following sections. With the rapid cooling produced by instantaneously delivered Ar distributed over the entire computational domain, the simulations have a compressed TQ time but a realistic CQ time (when compared with experiments). With the relatively cold, resistive CQ phase as the focus of the simulations it is possible to use physical,

Spitzer values of resistivity throughout these simulations, without any of the computational challenges that normally preclude realistic resistivity values in modelling the flat-top phase of high-performance tokamak plasmas using extended MHD codes.

As the MHD fields evolve, a test-particle module computes the guiding-centre-drift-motion of a trace population of REs. Four equations governing three spatial coordinates $[R, Z, \phi]$ and parallel velocity are integrated. Curvature, grad-B and $E \times B$ drift terms are included in the motion, with the relativistic factor γ multiplying the electron mass. The velocity equation includes acceleration by the electric field and slowing terms due to collisions, synchrotron and bremsstrahlung radiation. The component of velocity normal to the magnetic field is assumed based on a fixed pitch angle. In experiments, pitch angle can be inferred from measured synchrotron radiation [8], and such analysis of DIII-D RE beams finds a pitch angle of between 0.1 and 0.2. Therefore, a constant value of 0.15 is chosen in all simulations. No such measurement is available on C-Mod, but the same value is used in order to minimize the parameters that vary between simulations. The equations appear in the appendix.

The test REs are initiated with random positions and specified energies chosen to be somewhat above the runaway threshold, but not highly relativistic. Although the RE energies are evolved, a realistic energy distribution cannot be calculated without a kinetic model including RE generation mechanisms—particularly the avalanche, which continually produces new REs just above the RE threshold energy. The purpose of the test-particle model, therefore, is not to predict the RE energy distribution, or the total RE population, but to predict the effects of MHD fluctuations on the transport of high energy REs, as well as the strike points of escaping REs on the first wall. Kinetic Fokker–Planck modelling of RE populations during DIII-D disruptions has been performed by Harvey *et al* [9]. However, this model accounts for radial transport of REs using a diffusive (Rechester–Rosenbluth [10]) model with assumed fluctuating field amplitudes. In the first place, high energy REs are expected to exhibit reduced transport in the presence of fluctuating fields due to their large curvature drift [11]; second, the fluctuating field amplitude, $\delta B_r/B$, is unlikely to be uniform in space or constant in time during a disruption. Our MHD-plus-test-particle modelling is intended to address these limitations in simplified transport models and is thus complementary with Fokker–Planck modelling for understanding the behaviour of REs in tokamak disruptions.

4. Computational results

4.1. DIII-D simulations and effects of plasma shape

Two DIII-D rapid shutdown simulations were performed in which a broad radial profile of neutral Ar (slightly peaked in the core) is deposited at $t = 0$ to produce a rapid radiative collapse of the plasma temperature. The Ar profile after pellet ablation in the DIII-D experiments is not known; the effects of varying Ar profile will be considered in the next section. The total Ar quantity is comparable to that contained in the Ar ice pellets used for the DIII-D experiments, which contain about 7 torr l of Ar atoms (on the order of a third to a half of the deuterium ion inventory). The initial equilibria for the two simulations are EFIT reconstructions of two DIII-D discharges—137611 and 140586—which have diverted and limited shapes, respectively (figure 2). The diverted plasma has H-mode profiles prior to Ar pellet injection, while the limited plasma is in L-mode, although shortly after the Ar deposition, all profiles are substantially perturbed (figure 2(*c*)). Both of these discharges produce RE current plateaus following Ar pellet injection. In each simulation, the resistivity is given by a temperature and $Z_{\rm eff}$ dependent Spitzer expression, where $T_{\rm e}$ in each case falls to just tens of eV within about 0.01 ms of the start of the simulation. A population of 1598 trace REs is initiated in each simulation, all with starting energies of 150 keV, and random poloidal and toroidal positions inside the closed flux region. Because REs quickly accelerate to MeV energies, results are not sensitive to this starting energy, which is chosen to be above the runaway threshold but not highly relativistic. The simulations include toroidal mode numbers $n = 0$–10.

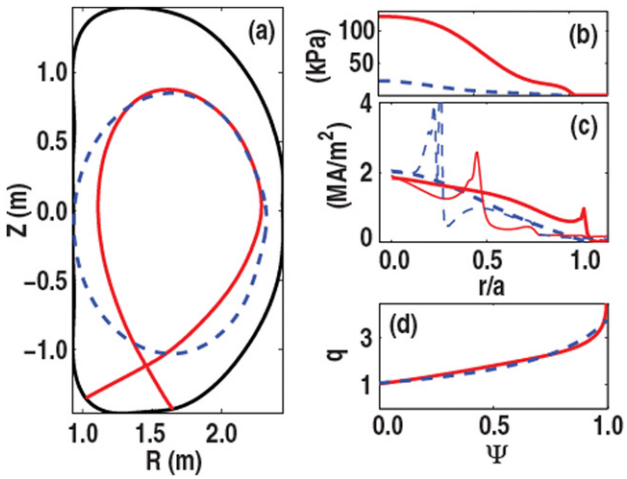

Figure 2. (*a*) Last closed flux surface shapes for the two DIII-D equilibria, reconstructed from shots 137611 (solid) and 140586 (dashed), (*b*) pressure profiles and (*c*) current density profiles (heavy lines are $t = 0$, narrow lines are $t = 0.17$ ms) for each versus normalized minor radius, and (*d*) q profiles versus normalized poloidal flux.

In both simulations, the pressure quickly becomes negligible and the current density profile evolves well away from its starting point prior to the onset of MHD (figure 2(*c*)). The evolution the current density profile is certainly dependent on the initial profile, but the MHD instabilities are governed by the stability properties of the significantly perturbed current density profile, and not those of the initial current density or pressure profiles. In the diverted simulation (figure 3), the contraction of the current density profile that follows the radiative cooling triggers the onset of MHD instabilities dominated by toroidal mode numbers $n = 1, 2$ and 3. The magnetic fields become stochastic over a significant region of the poloidal cross section, with some islands remaining intact in the core. In a narrow time window (∼0.2 ms) centred at about 0.8 ms from the start of the simulation, 32% of the initial RE population is lost. These REs strike the wall in a poloidally localized, but toroidally symmetric pattern at the outer divertor strike point. The outer (as opposed to inner) divertor is the logical strike point for REs travelling in the counter-current, co-B-field direction. The average energy of

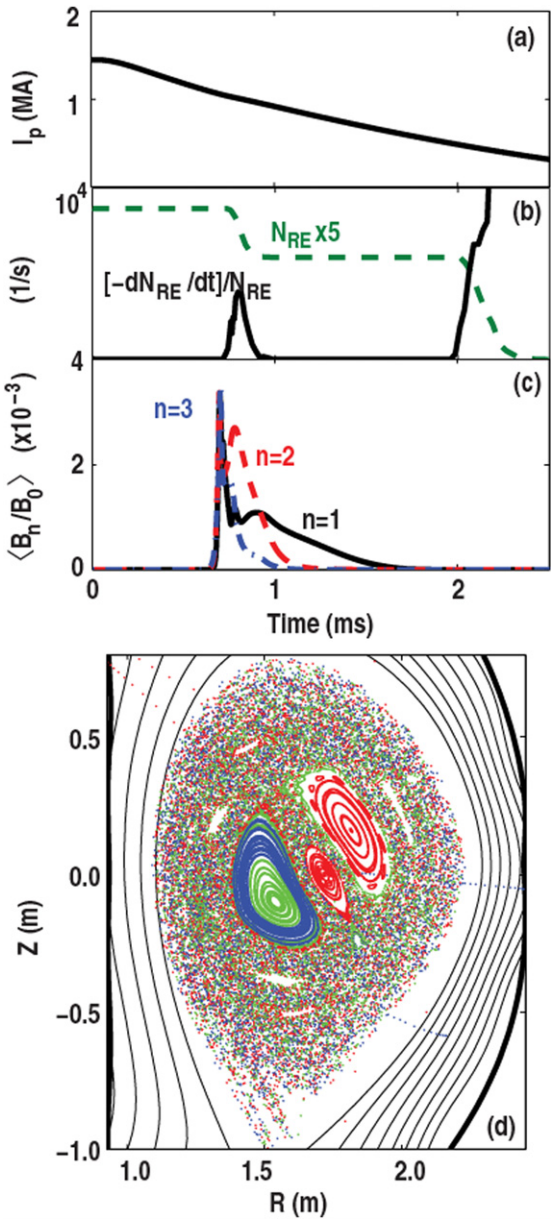

Figure 3. The diverted DIII-D simulation: time histories of (*a*) plasma current, (*b*) total number of confined REs (×5, dashed) and loss rate of REs (solid) and (*c*) amplitudes of the $n = 1$, 2 and 3 modes relative to $n = 0$, (*d*) Poincaré plot showing magnetic topology at 0.8 ms.

the escaping REs is 13 MeV, while the average energy of the remaining confined REs is 22 MeV just after the losses occur. The total CQ time for the simulation is close to 3 ms, but at 2 ms the remaining population of REs begins to escape due to the significant reduction in the confining plasma current. Although the flux surfaces have completely rehealed by this time, as the plasma current approaches zero, the confinement of all particles will of course be lost. In DIII-D discharge 137611, the decay of the plasma current effectively ceased when the remaining plasma current was entirely runaway current, and the REs remained confined much longer. Since we do not include the runaway current itself in our MHD equations, the model is most valid in the early CQ phase, before the RE current becomes an appreciable fraction of the total.

In the limited simulation, the MHD activity triggered by the radiative cooling has a different character from the diverted plasma. The dominant mode numbers are $n = 1$ and $n = 2$ (figure 4(*c*)), where the RE losses are associated with the second of two peaks in the $n = 1$ mode amplitude. A total of 11% of the initial REs are lost over a longer period between 0.6 and 1.5 ms. The escaping REs strike near the limiting point on the inner wall, in a toroidally asymmetric, rotating $n = 1$ pattern (figure 4(*b*)). DIII-D has a set of HXR detectors located at the outer midplane at five toroidal positions. HXRs are detected when high energy REs strike the first wall. Figure 4(*e*) shows the HXR pattern detected during shot 140586 shortly after the Ar pellet is injected. A similar rotating $n = 1$ pattern appears. Note, however, that data on the right side of figure 4 is plotted for a 2 ms time interval, compared with a 1 ms interval for the simulation results; hence, the rotation rates and length of the loss events differ by roughly that factor. Magnetic probes located at the outer midplane measuring $n = 1$ amplitude and phase at this time also show a larger amplitude $n = 1$ mode preceding the HXR bursts, followed by a smaller amplitude, rotating mode coincident with the HXRs (figure 4(*f*)). The initial, higher amplitude $n = 1$ mode that appears in the limited DIII-D simulation is a 1/1 mode accompanied by higher n harmonics, but produces stochasticity that is entirely localized to the core, leaving the outer flux surfaces intact (figure 5(*a*)). The second $n = 1$ mode has virtually no higher n harmonics and includes $m = 2$–6 components extending across the domain. But, there is little island overlap producing minimal stochasticity.

4.2. C-Mod simulations and effect of impurity deposition profile

Although C-Mod RE experiments are performed with MGI, where the impurities penetrate initially only into the edge, the C-Mod simulations are designed to isolate differences between the target plasmas in the two devices from differences in the fuelling methods. Hence, we perform two C-Mod simulation having different Ar deposition profiles (figure 6). In the first, the Ar profile is slightly peaked in the core, just as in the DIII-D simulations. The second profile contains the same total Ar quantity, but is peaked at the edge. The edge-peaked profile is more similar to MGI, but note that the Ar density in the core, and hence the cooling of the core, prior to MHD onset, is still greater than a true MGI-like scenario, where nearly all of the Ar would be localized to the edge. In the simulation, the enhanced cooling of the core provides significant numerical advantages relative to a plasma that remains in the keV range until the onset of MHD. Both simulations begin with the same diverted equilibrium, and with 1098 randomly seeded REs at 150 keV.

Similar to the DIII-D diverted simulation, the strong cooling of the core in the core-peaked simulation leads to contraction of the current density profile (figure 6(*d*)) and the onset of MHD instabilities with dominant $n = 2$ and $n = 1$ modes, including a 1/1 component (figure 7(*a*)). This MHD event, occurring at 0.2 ms, produces stochasticity across most of the poloidal plane, and results in the loss of nearly 100% of the REs in the simulation (figure 7(*c*)). REs with energies in the range ∼5 –10 MeV are lost to the outer divertor strike point in a toroidally symmetric pattern. Higher energy REs (up to

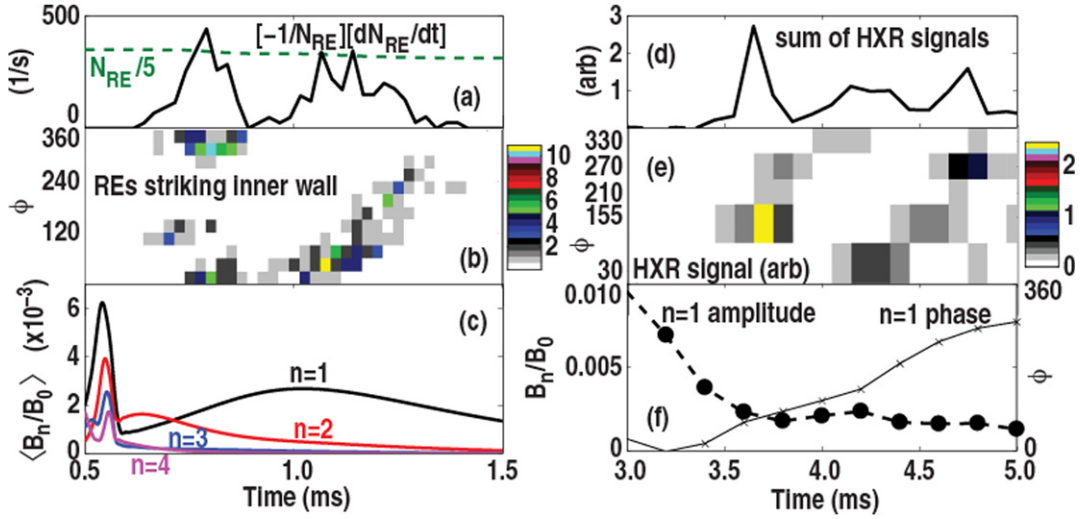

Figure 4. Left: limited DIII-D simulation showing (*a*) loss rate of REs between 0.5 and 1.5 ms (solid) and total N_{RE} divided by five (dashed), (*b*) toroidal distribution of RE strikes on the inner wall versus time, (*c*) amplitude of $n = 1$–4 modes relative to $n = 0$. Right: data from DIII-D shot 140586 showing (*d*) sum of signals on five HXR detectors at the midplane between 3.0 and 5.0 ms after pellet launch, (*e*) HXR signals at each toroidal location, and (*f*) amplitude and phase of $n = 1$ mode as measured by magnetic probes at the outer midplane.

∼20 MeV) strike the outer midplane due to large curvature drift producing outwardly displaced orbits. These REs strike the wall in a toroidally asymmetric pattern having $n = 2$ plus $n = 1$ symmetry corresponding the two largest modes (figure 8).

In the simulation with an edge-peaked Ar profile, less cooling of the core produces less significant contraction of the current profile. The first unstable mode to appear is a 4/3 mode just after 0.2 ms (figure 7(*b*)). A fraction of the REs—mainly in the edge—are lost at this time, but roughly half remain confined until the eventual onset of the 1/1 mode at 0.8 ms. Like in the core-peaked case, REs strike both the outer divertor and outer midplane, and REs striking the midplane during the first loss event exhibit the $n = 3$ symmetry of the dominant mode. In both C-Mod simulations, the number of confined REs eventually goes to zero as a direct result of MHD fluctuations. The time evolution of the core Ar concentration for each case is shown in figure 7(*d*). At the time of the 1/1 mode onset at 0.8 ms, the Ar quantity in the core increases for the initially edge-peaked case, indicating mixing due to advection associated with the mode. A second 1/1 event just after 1.2 ms further increased the core Ar until it is the same as in the initially core-peaked profile. The earlier 4/3 mode has no observable effect on Ar concentration in the core. In C-Mod high-Z MGI experiments, impurity mixing into the core, as evidenced by electron density measurements, is typically seen to occur over a short timescale following ∼1ms delay after the initial edge cooling. An example is figure 5(*b*) in [12], which shows density profiles from a neon MGI experiment. Given the numerous differences between the simulation presented here and the MGI experiments, only a qualitative comparison in this regard is reasonable.

The eventual loss of all REs in both C-Mod simulations clearly contrasts with the DIII-D results. Even with the same Ar fuelling profile, the diverted plasmas in the two devices produce quite different confinement results. This comparison points to a larger role for machine size or other equilibrium plasma parameters as the primary factor in the experimentally distinct RE observations, rather than the effects of MGI versus pellets.

4.3. ITER simulation and effects of machine size

A single ITER simulation is presented which has a diverted geometry (figure 9) and a core-peaked Ar profile that can be directly compared with the similar cases presented for DIII-D and C-Mod. Due to the larger number of poloidal grid points required for the ITER simulation, it includes only toroidal mode numbers $n = 0$ –5. Also, because of the higher initial core T_e (20 keV) the plasma takes longer to cool to numerically tractable levels. Hence, the Spitzer resistivity expression used is the same as in the other cases, except that the maximum T_e used in its evaluation is 300 eV; that is, the resistivity is enhanced in regions of the plasma that are above 300 eV, but becomes identical to Spitzer once the plasma is below 300 eV everywhere. The simulation is initiated with 2399 REs inside the closed flux region.

In figure 9(*c*) the amplitudes of the $n = 1$, 2 and 3 modes for the ITER simulation are shown throughout the 5.5 ms duration of the simulation. The modes first appear just before 1 ms and two distinct peaks appear in the dominant $n = 1$ mode as well as in the $n = 2$ mode at 1.05 and 1.3 ms. Throughout this MHD phase, no REs escape (figure 9(*d*)). Shortly after the $n > 0$ modes have disappeared, a gradual loss of REs at the largest minor radius begins. As in the DIII-D diverted simulation, these losses are associated with the decay of the confining current. At the times associated with the two MHD peaks, the outer flux surfaces remain largely intact, while large islands and stochastic regions appear only in the core (figure 10(*a*)).

Figures 9(*c*), 7(*a*) and 3(*c*) allow comparison of only the globally averaged amplitudes of the fluctuating fields for the diverted, core-peaked Ar simulation of each device. We can also calculate for each case the radial profile of $\delta B_r/B$ at the time when the global amplitude is maximum. In each simulation, $\delta B_r/B$ is peaked inside of $q = 1$ at that time,

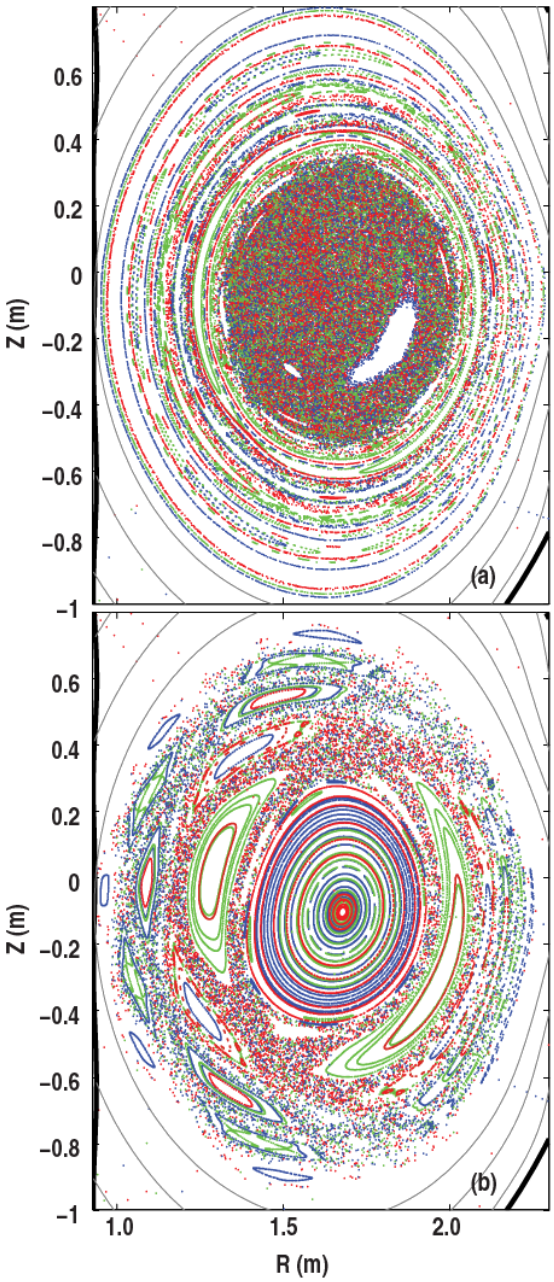

Figure 5. (*a*) Poincaré plot of magnetic fields at 0.54 ms in the limited DIII-D simulation, when the first $n = 1$ mode peaks. (*b*) Poincaré plot at 1.04 ms when the second $n = 1$ mode peaks.

with no systematic trend in the maximum amplitudes. Away from the peak however, a clear trend in the amplitudes with device major radius is found. In figure 11 the amplitude of $\delta B_r/B$ versus major radius at both $q = 1$ and $r/a = 0.8$ for the three simulations is plotted. At $q = 1$, the trend is slightly weaker than $1/R$, while further towards the edge, at $r/a = 0.8$, the amplitudes fall off slightly faster than $1/R$. In figure 12, we plot the RE confinement time ($\tau_{RE} = N_{RE}/[\mathrm{d}N_{RE}/\mathrm{d}t]$) versus major radius at its minimum value (when the magnetic fluctuations are largest) for each simulation except the ITER simulation, where no RE losses during the MHD phase occurred. The DIII-D diverted simulation exhibits a 25 times larger confinement time than the C-Mod simulation, which is very close to a factor of R^3.

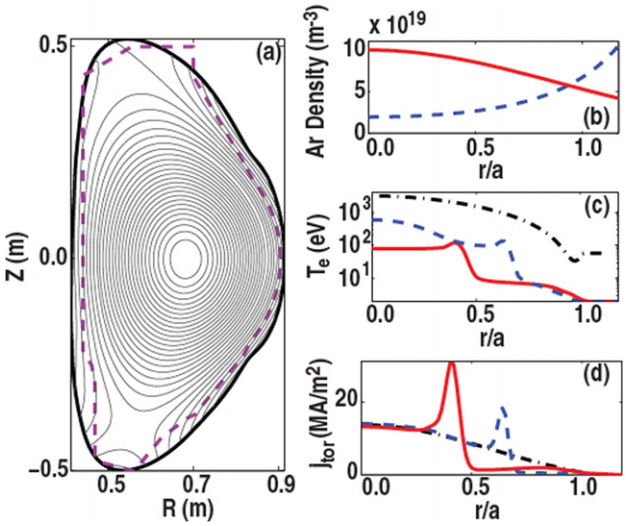

Figure 6. (*a*) Poloidal flux contours for Alcator C-Mod equilibrium used in the two simulations. Solid boundary is simulation boundary, dashed line is actual C-Mod first wall geometry. (*b*) Neutral Ar profiles at $t = 0$ for the core-peaked (solid) and edge-peak (dashed) C-Mod simulations. Temperature profiles (*c*) and current density profiles (*d*) at 0.1 ms (prior to MHD onset) are shown for both cases, along with the initial profiles (dashed–dotted).

5. Discussion and conclusions

Five extended MHD simulations have been performed of rapid shutdown scenarios in three tokamaks to investigate the effects of various experimental parameters on runaway electron confinement during the thermal-quench-induced MHD fluctuations. Due to certain simplifications, especially in the impurity delivery model and the runaway energy distribution, these results cannot be validated in all aspects against experiments on C-Mod and DIII-D, although certain experimental features are reproduced. The simulations should be viewed in part as numerical experiments designed to fill experimental gaps and to draw out certain trends that may be ambiguous in the data.

In two DIII-D simulations, the effects of plasma shape were examined by comparing an elongated, diverted plasma geometry with a lower elongation, limited plasma. Overall, the fraction of REs lost in the limited plasma was smaller than in the diverted plasma, which is consistent with the general experimental observation that limited plasmas confine REs better. However, perhaps more interestingly, the loss mechanism for the REs in the two configuration was essentially different. In the diverted case, stochastic fields extending across much of the domain caused REs to follow open field lines to the divertor. In the limited plasma, large stochastic regions never appeared, and the RE losses were entirely associated with an external $n = 1$ motion of the plasma into the centre column, producing a tell-tale $n = 1$ RE striking pattern. In the limited plasma, both the spatial localization of the first $n = 1$ mode, and the absent toroidal harmonics during the second $n = 1$ mode are unique features not observed in the diverted simulation, suggesting differences in the coupling between MHD modes may play a role in improved RE confinement.

The most significant feature of the two C-Mod simulations is that, despite the variation in Ar deposition profile and the

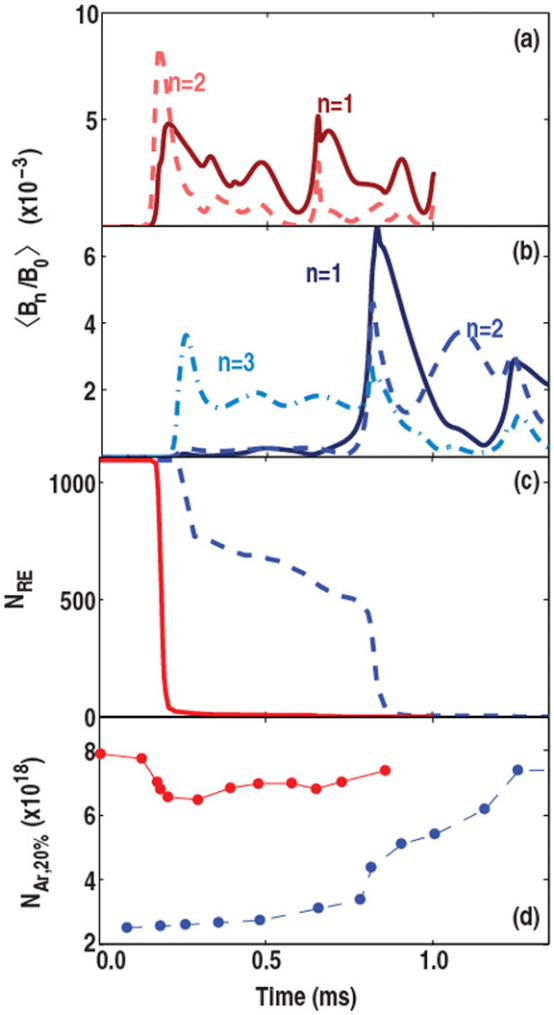

Figure 7. (*a*) Mode amplitudes of $n = 1$ and 2 versus time for the core-peaked C-Mod simulation, (*b*) mode amplitudes of $n = 1, 2, 3$ versus time for the edge-peaked simulation, (*c*) total number of confined REs versus time for core-peaked (solid) and edge-peaked cases (dashed), (*d*) total number of Ar ions inside 20% flux surface versus time for both C-Mod simulations.

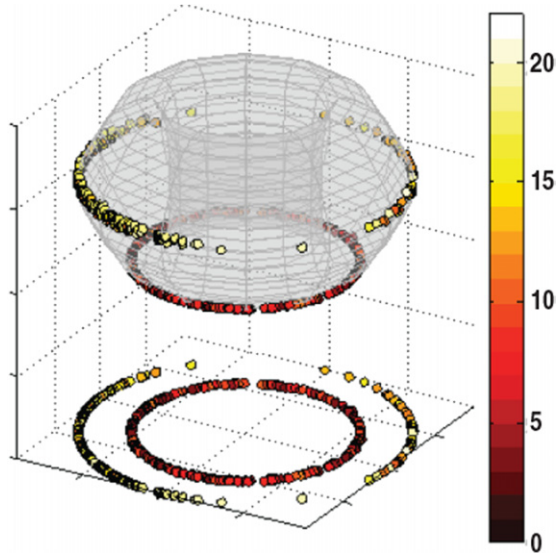

Figure 8. The distribution of RE strikes on the C-Mod boundary in 3D, and projection on a toroidal plane, for the core-peaked simulation. Colours are RE energies in MeV.

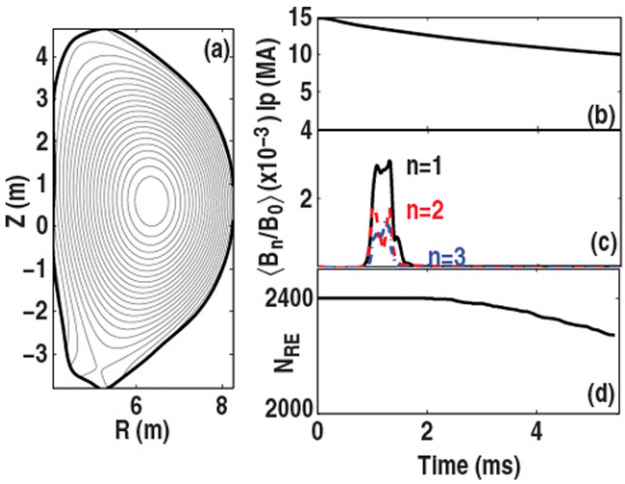

Figure 9. (*a*) Poloidal flux contours of the equilibrium used for the ITER simulations. Time evolution of (*a*) plasma current, (*b*) $n = 1, 2, 3$ mode amplitudes, and (*c*) total number of confined REs.

resulting MHD sequence, the eventual loss of REs due to MHD was 100% in each case, in stark contrast with DIII-D. A comparison of the two cases does point to some differences between pellet and MGI experiments, although cooling is more strongly localized to the edge in MGI than the edge-peaked Ar simulation presented here. Previous MGI simulations with edge cooling only [13] have suggested that a $2/1$ mode initiates the core TQ, followed by a $1/1$ mode that ultimately collapses the temperature on axis. In the simulation presented here, a mode closer to the core (4/3) appeared first, but the basic paradigm of an initial mode outside $q = 1$ and a delay before the $1/1$ onset holds. The key finding regarding RE transport is that the REs in the core remain confined until the $1/1$ mode appears. The same $1/1$ mode appears to efficiently mix Ar impurities from the edge into the core.

Comparison of C-Mod, DIII-D and ITER simulations points to a machine-size trend. Each machine is roughly a factor of three larger in major radius than the previous, and the fraction of REs lost due to MHD for the three devices is 100%, 32% and 0% respectively. To be sure, we cannot unambiguously isolate the effect of major radius from other equilibrium properties that may affect RE confinement, such as shape, initial profiles and proximity of the wall. A further study with identical size-scaled equilibria could more definitively address this issue, but is left for future work.

The retention of good flux surfaces at the edge during the MHD event in ITER appears responsible for the perfect RE confinement found in the simulation. The low fluctuating field amplitude ($\delta B_r/B \sim 10^{-4}$) in the edge is consistent with a $1/R$ trend in the edge fluctuations over all three devices. Given a $1/R$ scaling for $\delta B_r/B$, the factor of R^3 variation in the RE confinement time between C-Mod and DIII-D agrees with a Rechester–Rosenbluth [10] scaling for diffusion on stochastic fields:

$$D \propto R\left(\frac{\delta B_r}{B}\right)^2 \propto \frac{1}{R}; \qquad \tau_{RE} \propto R^2/D \propto R^3. \quad (1)$$

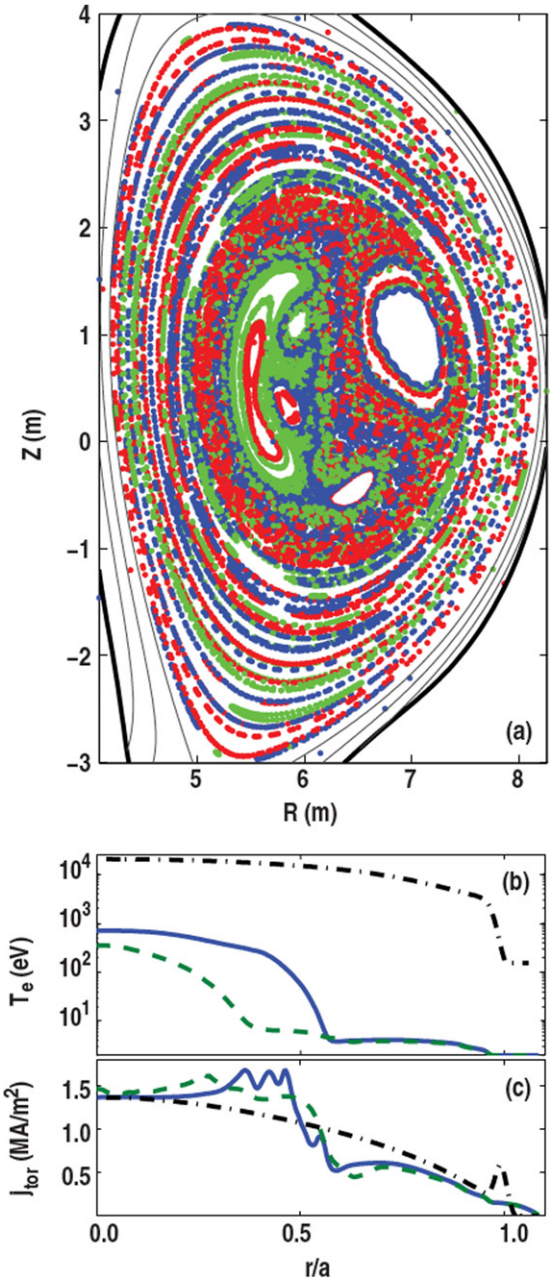

Figure 10. (*a*) Poincaré plots of magnetic field lines in the ITER simulation at 1.30 ms, (*b*) electron temperature profiles (on a log scale) at $t = 0$, (dashed–dotted) 1.05 ms (solid) and 1.3 ms (dashed), and (*c*) current density profiles at the same three times.

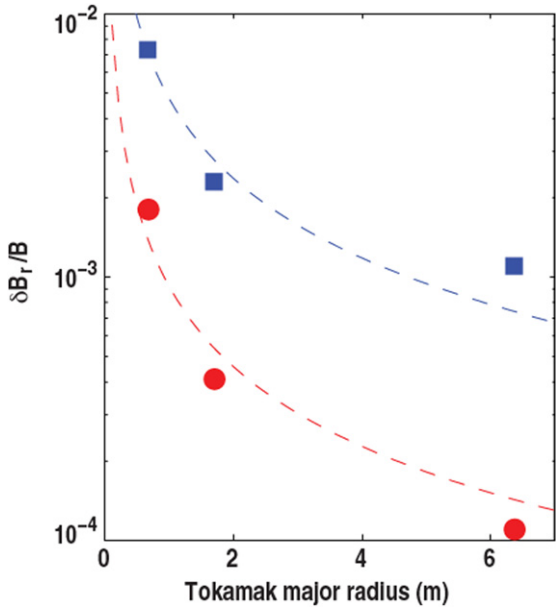

Figure 11. Fluctuating field amplitudes ($\delta B_r/B$) for all three tokamaks with diverted geometry and core-peaked Ar at $q = 1$ (squares) and $r/a = 0.8$ (circles). Dashed curves are proportional to $1/R$.

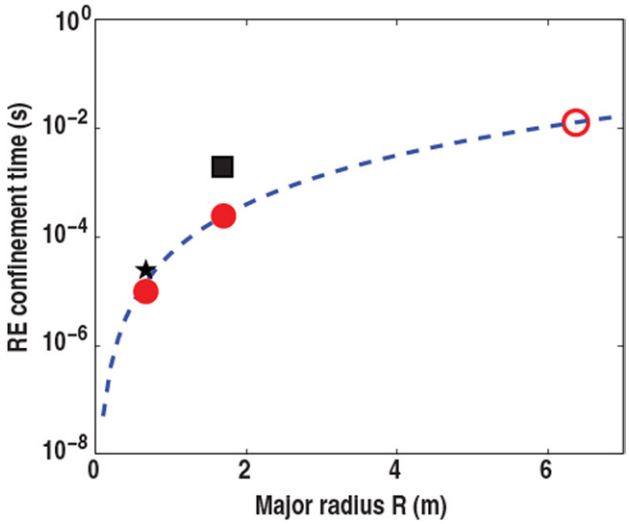

Figure 12. RE confinement time for each simulation when the RE loss rate is maximum. Solid circles are the diverted, core-peaked simulations of C-Mod and DIII-D. Dashed curves are proportional to R^3. The open circle is the extrapolation of the trend to ITER (where no RE losses occurred). The star is the edge-peaked C-Mod simulation, and the square is the limited DIII-D simulation.

Since the magnetic fluctuations last only a short time before the flux surfaces reheal, a comparison of the RE confinement times with the duration of the fluctuations in each case is also illustrative. The fluctuation duration increases with major radius, but only about linearly. In particular, DIII-D has a duration which is comparable to its RE confinement time (tenths of a ms), while the C-Mod RE confinement time is short compared with the MHD duration, and the extrapolated 10 ms τ_{RE} in ITER is much longer than the duration of the MHD modes in that simulation. The total RE loss in C-Mod, partial loss in DIII-D and zero loss in ITER are perhaps in large part explained by this comparison. The C-Mod results also agree with the experimental finding that no observable fraction of the seed is retained after the TQ in diverted plasmas [6]. The experimental finding in DIII-D diverted plasmas is the highly unreliable appearance of post-TQ runaways on a shot-to-shot basis [3]. The DIII-D simulations suggest the device occupies a regime of marginal RE confinement based on the comparison of relevant time scales and the partial loss of seed REs, which is entirely consistent with the experimental finding. But the precise details of why certain diverted DIII-D discharges confine more REs than others demand further studies with multiple DIII-D diverted equilibria to adequately address.

The single ITER simulation finds very good confinement of REs during disruptive MHD activity due to retention of good flux surfaces in the edge. Further simulations with more realistic impurity fuelling models may somewhat alter these results, in particular due to the excitation of edge modes. However, the size scaling suggested by comparing simulations of three devices bodes poorly for the possibility of significant RE seed loss to prevent an RE avalanche during the CQ in ITER. Although each present-day tokamak has, for the most part, performed unique RE experiments, making direct cross-device comparison difficult, some experimental trends appear to support the basic finding of improved confinement for larger device sizes. In addition to the C-Mod and DIII-D results already discussed, we note that JET experiments with high-Z (Ne or Ar) MGI (and no deliberate RE seed, such as with LHCD) routinely produce RE current plateaus [14]. Both C-Mod and DIII-D have performed high-Z MGI experiments [4, 5] in diverted plasmas, but unlike the larger JET, neither produce RE current plateaus.

Acknowledgments

This work was supported by the US Department of Energy under DE-FG02-95ER54309, DE-FG02-07ER54917 and DE-FG02-04ER54762. This research used resources of the National Energy Research Scientific Computing Center, which is supported by the Office of Science of the US Department of Energy under Contract No DE-AC02-05CH11231.

Appendix. Electron orbit equations

The orbits of the fast electrons are governed by equations (A1)–(A3), which include $E \times B$, grad-B and curvature drift. A large aspect ratio approximation is used in the drift terms to avoid calculating differentials of the magnetic field at every MHD time step:

$$\mathrm{d}R = \frac{v_\parallel B_R}{B}\mathrm{d}t + \frac{1}{B^2}[\vec{E}\times\vec{B}]_R\,\mathrm{d}t, \tag{A1}$$

$$\mathrm{d}Z = \frac{v_\parallel B_Z}{B}\mathrm{d}t + \frac{1}{R}\frac{\gamma m_\mathrm{e} v_\perp^2}{2eB}\mathrm{d}t + \frac{1}{R}\frac{\gamma m_\mathrm{e} v_\parallel^2}{eB}\mathrm{d}t + \frac{1}{B^2}[\vec{E}\times\vec{B}]_Z\,\mathrm{d}t, \tag{A2}$$

$$\mathrm{d}\phi = \frac{v_\parallel B_\phi}{RB}\mathrm{d}t + \frac{1}{RB^2}[\vec{E}\times\vec{B}]_\phi\,\mathrm{d}t. \tag{A3}$$

The electric field is given by the resistive-MHD Ohm's law $\vec{E} + \vec{v}\times\vec{B} = \eta\vec{j}$, where the velocity, magnetic field and current density are calculated at each MHD time step. The velocity perpendicular to the magnetic field, $v_\perp$, is given by a fixed pitch-angle assumption, $\theta = v_\perp/v_\parallel = 0.15$. The velocity parallel to the magnetic field is evolved according to the equation:

$$\begin{aligned}\mathrm{d}v_\parallel = &-\frac{eE_\parallel}{\gamma^3 m_\mathrm{e}}\mathrm{d}t + \frac{v_\perp^2}{\gamma^2}\frac{B_R}{2BR}\,\mathrm{d}t \\ &- \frac{1}{\gamma^4}\frac{v_\parallel}{|v_\parallel|^3}\frac{e^4\ln\Lambda}{4\pi\varepsilon_0^2 m_\mathrm{e}^2}n_\mathrm{e}(Z_\mathrm{eff}+1+\gamma)\,\mathrm{d}t \\ &- \gamma v_\parallel^3\frac{e^2}{6\pi\varepsilon_0 m_\mathrm{e}c^3}\left(\frac{1}{R_0^2}+\frac{e^2B^2v_\perp^2}{\gamma^2 m_\mathrm{e}^2 v_\parallel^4}\right)\mathrm{d}t \\ &- \frac{1}{\gamma^2}\frac{e^4(Z_\mathrm{eff}+1)}{548\pi^2\varepsilon_0^2 m_\mathrm{e}^2c^2}n_\mathrm{e}\left(\ln(2\gamma)-\frac{1}{3}\right)\frac{v_\parallel}{|v_\parallel|}\mathrm{d}t.\end{aligned} \tag{A4}$$

The final three terms in (A4) are the drag terms due to collisions, synchrotron radiation and bremsstrahlung, respectively. Each of these expressions is taken from Bakhtiari *et al* [15]. In these simulations of the high electric field phase that precedes the runaway plateau phase, the E-field acceleration tends to dominate all other terms, with synchrotron drag sometimes becoming significant at the end of the simulation as the E-field drops and γ becomes large. Nevertheless, we will discuss and estimate the size of each term in the present simulations. For comparison we will first evaluate the E-field acceleration term for DIII-D. In the short time before the electric field reaches its maximum value ($\sim$100 V m^{-1}), the REs accelerate to $\gamma \approx 3.5$, and the E-field acceleration term reaches its maximum magnitude of about 10^{12} m s^{-2}. By the end of the simulation, the E-field has dropped due to the lower current density and reduced Z_eff, and the surviving REs have accelerated as high as $\gamma = 100$ (about 50 MeV), so that the acceleration has decreased to just under 10^7 m s^{-2}.

The collisional term includes contributions from both collisions with ions, which should scatter the pitch angle but conserve energy, and with electrons, which have an associated energy loss [16]. Since a fixed pitch angle is assumed here, pitch-angle scattering contributions result in an artificial loss of RE energy. The Z_eff + 1 portion of the term (associated with pitch-angle scattering [16]) can obtain values on the order of 10^{11} early in the simulation when $\gamma \sim 1$, assuming the maximum Z_eff of 7 obtained after the initial ionization of the Ar. At $\gamma = 100$, this term is smaller than 10^3. The other portion of the term which is proportional to γ is initially the smaller term, but eventually becomes dominant. Still, excepting the first 0.1 ms of the simulation before the E-field rises, the total collisional term is always two or more orders of magnitude smaller than the E-field acceleration.

The synchrotron radiation drag term includes contributions from both the motion around the major radius of the torus and the gyro-motion, which produces a force along the helical direction of motion and thus contributes to the parallel drag [17]. In fact, the gyro-motion contribution is always the larger of the two terms in brackets and would become smaller only at γ values of several hundred. The inclusion of pitch-angle scattering in the calculations would enhance the effect of synchrotron drag from the gyro-motion [17], which is proportional to the pitch-angle squared. Overall, synchrotron term initially obtains values of nearly 10^7 at $\gamma \sim 1$ and falls off linearly with γ.

The bremsstrahlung term, like the collisional term, increases with Z_eff and electron density, but is also small. Initial values in these simulations (again using $Z_\mathrm{eff} = 7$) are

on the order of 2×10^7 at $\gamma \sim 1$, dropping to below 10^4 at $\gamma \sim 100$. In shutdown scenarios where the E-field is smaller or the injected impurity density is larger, bremsstrahlung can be an important factor in limiting RE energy [15], but the Ar pellets modelled here do not contain enough material to achieve that parameter regime.

As with pitch-angle scattering, the second term in (A4)—the mirror force—also does not conserve energy properly when a fixed pitch angle is assumed. However, the term changes sign every half poloidal transit (all particles are passing), and therefore tends to average to zero. We can easily estimate the change in energy due to this term before it switches sign. Assuming $q = 2$ and $\gamma = 20$ (about 10 MeV), $\delta v_\parallel$ for one half poloidal transit is approximately $10^5\,\mathrm{m\,s^{-1}}$ (this is the same for each device since the term varies inversely with R but the poloidal transit length increases as R). In that case γ would vary between 18 and 20 over the full poloidal orbit, or about 10% in energy. We have directly tested the effects of omitting this term on the results by repeating the diverted DIII-D simulation without it. The average energies of the runaway populations differ by less than 3.5% between the two cases over the entire 2 ms prior to the final loss event. The fraction of REs lost during the MHD event increases by less than 2% with that term excluded.

The magnitudes given for each term were specifically for DIII-D; however, the size of each term is tracked for every RE orbit integrated over the length of the calculations. A comparison of REs for each device shows very similar amplitudes versus time for every term in (A4), with the E-field acceleration always large compared with the others. Because the REs remain confined the longest in ITER they reach the highest γ values (over 200); at the same time the E-field remains somewhat lower in the ITER case through the late phase of the simulation. Consequently, those REs show an appreciable drag effect from synchrotron radiation, with no other term making a significant contribution.

Ideally, a more accurate RE energy model including the evolution of $v_\perp$ will be included in future simulations. However, as discussed in the last paragraph of section 3, the primary purpose of this modelling is not to predict the RE energy distribution, but the comparative effects of various equilibrium parameters on RE confinement. The lack of an avalanche RE generation model, which would produce an exponential RE energy distribution [1] (rather than the nearly mono-energetic populations in these simulations), is almost certainly the largest source of discrepancy with reality.

References

[1] Jayakumar R. *et al* 1993 *Phys. Lett.* A **172** 447
[2] ITER Physics Expert Group on Disruptions, Plasma Control, and MHD, ITER Physics Basis Editors: Chapter 3: MHD stability, operational limits and disruptions 1999 *Nucl. Fusion* **39** 2251
[3] Commaux N. *et al* 2011 Novel rapid shutdown strategies for runaway electron suppression in DIII-D *Nucl. Fusion* submitted
[4] Hollmann E.M. *et al* 2008 *Nucl. Fusion* **48** 115007
[5] Granetz R.S. *et al* 2007 *Nucl. Fusion* **47** 1086
[6] Marmar E. *et al* 2009 *Nucl. Fusion* **49** 104014
[7] Sovinec C.R. *et al* 2004 *J. Comput. Phys.* **195** 355
[8] Jaspers R. *et al* 2001 *Rev. Sci. Instrum.* **72** 466
[9] Harvey R.W. *et al* 2000 *Phys. Plasmas* **7** 4590
[10] Rechester A.B. and Rosenbluth M.N. 1978 *Phys. Rev. Lett.* **40** 38
[11] Mynick H.E. and Strachan J.D. 1981 *Phys. Fluids* **24** 695
[12] Izzo V.A. *et al* 2008 *Phys. Plasmas* **15** 056109
[13] Izzo V.A. 2006 *Nucl. Fusion* **46** 541
[14] Lehnen M. *et al* 2009 *Proc. 36th EPS Conf. on Plasma Physics (Sofia, Bulgaria, 29 June–3 July 2009)* http://www.iop.org/ Jet/fulltext/EFDC090636.pdf
[15] Bakhtiari M. *et al* 2005 *Phys. Plasmas* **12** 102503
[16] Fussmann G. 1979 *Nucl. Fusion* **19** 327
[17] Andersson F., Helander P. and Eriksson L.-G. 2001 *Phys. Plasmas* **8** 5221